Time-dependence of subsidence above a producing gas reservoir with salt top seal: A finite element model study of the role of salt flow

George Marketos, Taco Broerse, Christopher J. Spiers, and Rob Govers

ABSTRACT

Numerous producing and actively subsiding gas fields worldwide have salt top seals, but surface subsidence records exist for very few. This paper summarizes both reservoir pore pressure data and subsidence measurements obtained for a salt-sealed gas field in northern Europe. The data indicate a time dependence in subsidence evolution, with subsidence rates remaining relatively constant, while pore pressure depletion rates decrease. The creep of the thick, overlying salt may play a part in causing this time-dependence. The present work assesses salt creep flow's role in controlling the evolution of subsidence through finite element models. Salt creep effects are investigated in isolation, and independently of other factors, incorporating uncertainty in salt flow mechanisms and rheology. Comparing model results with field subsidence measurements suggests that salt flow can account for part of the time-dependent subsidence observed but cannot fully explain the field data, a finding that is also potentially important for other salt-sealed reservoirs around the world. Another important conclusion of the current study is that additional mechanisms that can lead to time-dependent subsidence must be active in the field studied.

INTRODUCTION

The present study focuses on a medium-sized natural gas field composed of a salt-capped, approximately 100-m-thick sandstone reservoir situated in the Netherlands (see Fokker et al., 2018 for a concise review of subsidence in the Netherlands). The reservoir is located as

Manuscript received October 25, 2020; provisional acceptance March 23, 2021; revised manuscript received July 28, 2021; final acceptance August 1, 2023; preliminary ahead of print version published November 15, 2025.
DOI:10.1306/11122520175

AUTHORS

GEORGE MARKETOS ~ *COWI U.K., London, United Kingdom; g.marketos.99@cantab.net*

George Marketos is a geomechanics consultant with expertise in modeling the complex response of geomaterials for engineering applications. He holds a Ph.D. from Cambridge University's Geotechnical and Environmental Research Group (2007) and has since worked as a researcher at the United Kingdom's National Oceanography Center, at Imperial College London, and at Utrecht University. He is the author of more than 20 peer-reviewed international publications on modeling of complex geomaterials response as affected by the mechanics at the micro scale and topics that range from wave propagation through soil and rock to salt creep flow. As a practicing geo-engineer, he has worked for United Kingdom-based firms Tony Gee and Partners and COWI and is currently based in Greece, where he continues his work for COWI as a consultant on numerical modeling for complex geomechanics and underground works or for prediction of underground systems response. In parallel, he is very active in code development and validation, doing research and development on novel geomaterials modeling techniques and methods.

TACO BROERSE ~ *Faculty of Civil Engineering and Geosciences, Delft University of Technology, Delft, the Netherlands; D.B.T.Broerse@tudelft.nl*

Taco Broerse is an assistant professor in the Department of Geoscience and Remote Sensing, Faculty of Civil Engineering and Geosciences, at Delft University of Technology. His research focuses on modeling and observing deformation of the Earth's surface, in response to tectonic and isostatic processes, as well as anthropogenic activities in the subsurface.

CHRISTOPHER J. SPIERS ~ *Department of Earth Sciences, Utrecht University, Utrecht, the Netherlands; C.J.Spiers@uu.nl*

Chris J. Spiers is emeritus professor at the High Pressure-Temperature (HPT) Laboratory in the Geosciences Faculty at Utrecht University. He led the laboratory as professor of earth materials until 2020,

specializing in experimental rock and fault mechanics and effects of fluids. He gained his Ph.D. from Imperial College, London. Following a Miller Fellowship at University of California, Berkeley (1980–1981), he moved to Utrecht, where he built up the HPT Laboratory, receiving his chair in 1992. He has worked on topics from creep of crustal and upper mantle rock materials to seismic fault friction and to deformation of reservoir rocks, cap rocks, coal, and shales. He has served as dean and education director in earth sciences at Utrecht and played a leading role in university and national research programs on geo-resources and geo-storage. He has published more than 220 peer-reviewed papers and book contributions, including some 40 papers on rock salt deformation and transport properties. In 2017, he received the European Geosciences Union Néel Medal for his contribution to Rock Physics.

ROB GOVERS ~ *Department of Earth Sciences, Utrecht University, Utrecht, the Netherlands; R.Govers@uu.nl*

Rob Govers is an associate professor in the Geophysics Group at Utrecht University's Geosciences Faculty. He has been leading the Tectonophysics research team since 2012. He earned his Ph.D. from Utrecht University and completed a postdoctoral fellowship with the Geodynamics Research Group at Penn State before joining the Tectonophysics research team in 1995. His research uses high-performance computing to tackle various problems, including Bayesian inference of earth processes and rheological properties, the earthquake cycle, and geomechanical issues related to geo-resources and storage, such as subsidence. He has served as an expert advisor for Dutch parliamentary committees on hazards associated with the Groningen gas field, as an editor-in-chief for the journal *Tectonophysics*, and on committees for the Dutch Research Council. He is often featured in the news for his insights on recent natural disasters. He has published more than 70 peer-reviewed papers and book chapters, which have been cited more than 5500 times. In 2014, he was awarded a fellowship by the Geological Society of America.

shown in Figure 1 at a depth of approximately 3400 m. Production started in 1986 and has continued for almost 35 yr, so that reservoir pressure is now substantially depleted. Measurements of surface subsidence have been collected more or less since the start of production and continue to this day. The extensive data set obtained up to 2015 is used to assess the contribution of salt flow to subsidence evolution.

The current study focuses on this specific gas field, as production-induced surface subsidence displays an anomalous time-dependent behavior that is not proportional to reservoir pore pressure decrease in the manner expected for a geomechanical system obeying a linear (elastic) response to pore pressure changes (see Figure 2). The present work was conducted at Utrecht University as part of a larger, multipartner research project funded by the field operator (Nederlandse Aardolie Maatschappij [NAM]). Several mechanisms that are potentially responsible for the time-dependent subsidence were tested in isolation of each other to determine which ones were relevant. All of the work (including data, results, and conclusions) presented here is openly available online for scrutiny by the public and regulator (see https://www.nam.nl/gas-en-oliewinning/wadden/onderzoeksrapportages-wadden.html) as part of the output of the overall project. The present peer-reviewed journal paper presents a concise summary of the Utrecht University results for the specialist international scientific community.

Here, the focus lies entirely on modeling one source of time-dependence (i.e., one subsidence evolution mechanism), that of time-dependent displacements induced by creep inside the salt layer that caps the reservoir. The principle behind the salt creep flow hypothesis is that gas production causes reservoir stress changes and compaction, which lead to the development of shear stresses within the salt. The salt, which behaves over time as a viscoelastic material, flows to relax these shear stresses and produces time-dependent ground displacements, the ground surface manifestation of which is time-evolving subsidence (Marketos et al., 2015b, 2016).

The aim here is to assess (by comparison of modeled versus measured subsidence) what proportion of the subsidence observed above the studied reservoir can be attributed to salt creep flow and identify whether other mechanisms may be responsible for the anomalous time-dependence of observed subsidence. Understanding which mechanisms lead to subsidence is of key importance to improving subsidence modeling and increasing confidence in subsidence predictions that otherwise rely on empirical extrapolation of trends measured to date. Note that subsidence with a time-delay occurs over several other fields throughout the world sealed by salt (Hettema et al., 2002).

This study uses the finite element method to investigate salt flow, as done in a number of previous numerical modeling studies (e.g., Breunese et al., 2003; Orlić and Wassing, 2013; Li and Urai, 2016). More specifically, the analyses use the GTECTON finite element code (Govers et al., 2014). Two-dimensional (2-D)

axisymmetric (i.e., pseudo-three-dimensional [pseudo 3-D] with rotational symmetry and full 3-D finite element models presented here incorporate key aspects of the field's complexity. Analysis results are compared with field measurements of subsidence. The faster-running, axisymmetric models, which form the majority of analyses, allow one to explore the effects of uncertainties in salt creep model parameters cost-effectively and efficiently. The full 3-D approach (which incorporates the effects of lateral variations in material layer thickness and more accurately accounts for spatial-temporal variations in reservoir pore pressure history) is then used to confirm the observed subsidence trends in the axisymmetric runs, validating their conclusions.

GAS FIELD DATA

Geological Setting

The natural gas field studied here is situated in the Netherlands, as shown in Figure 1. The gas bearing stratum is the approximately 100-m-thick Rotliegend sandstone layer at a depth of approximately 3400 m. This is overlain by a claystone (the Ten Boer) formation and capped by the Zechstein evaporite (mostly halite) sequence, which at this location is more than 1000 m thick. The reservoir is underlain by locally coal-bearing Carboniferous shales and siltstone source rocks. A cross section through the geological model is given in Figure 3. The sedimentary sequence (including the reservoir rock) is near-horizontal and includes faults and permeability variations that bound the gas-producing area to that shown in Figure 1B.

Reservoir Pore Pressure History

The gas field's operating company (NAM) kindly provided data on the spatial and temporal variations of pore pressures in the Rotliegend sandstone reservoir unit of the gas field (see Figure 1B). These data represent the output of a pore-fluid pressure analysis (conducted by NAM) based on pore pressure measurements at wells and constitute one possible pore pressure distribution out of many alternative scenarios investigated by NAM (Nederlandse Aardolie Maatschappij, 2017). Figure 1B includes the plan view of the disc-shaped reservoir (bold black circle) that is used to approximate the field extent in the axisymmetric analyses and calculate the mean pressures shown in Figure 4. Although the reservoir extent and shape are much more accurately represented in the 3-D analyses described in this manuscript, it will be shown that these details' inclusion does not change the model subsidence trends in a qualitative sense.

Figure 4 plots the evolution of the change in minimum and mean reservoir pore pressure since the start of gas production, as derived from the above-mentioned pore pressure data supplied by NAM. In 1986, the minimum reservoir pore pressure was 49 MPa, decreasing to 4 MPa in 2014. The average pore pressure inside the

ACKNOWLEDGMENTS

The authors would like to thank Nederlandse Aardolie Maatschappij (NAM) for funding this work and for providing the data that are presented in Figures 1B, 2–5, 10, and 11. Note again that the subsidence data and present results are all openly available to the public at https://www.nlog.nl/ and via https://nam-feitenencijfers.data-app.nl/download/rapport/ee804e7a-f0c1-4ea1-a98b-50e4e4fa8f9a?open=true. Helpful discussions with Antony Mossop, Rob van Eijs, Dirk Doornhof, and Hermann Baehr of NAM/Shell are gratefully acknowledged.

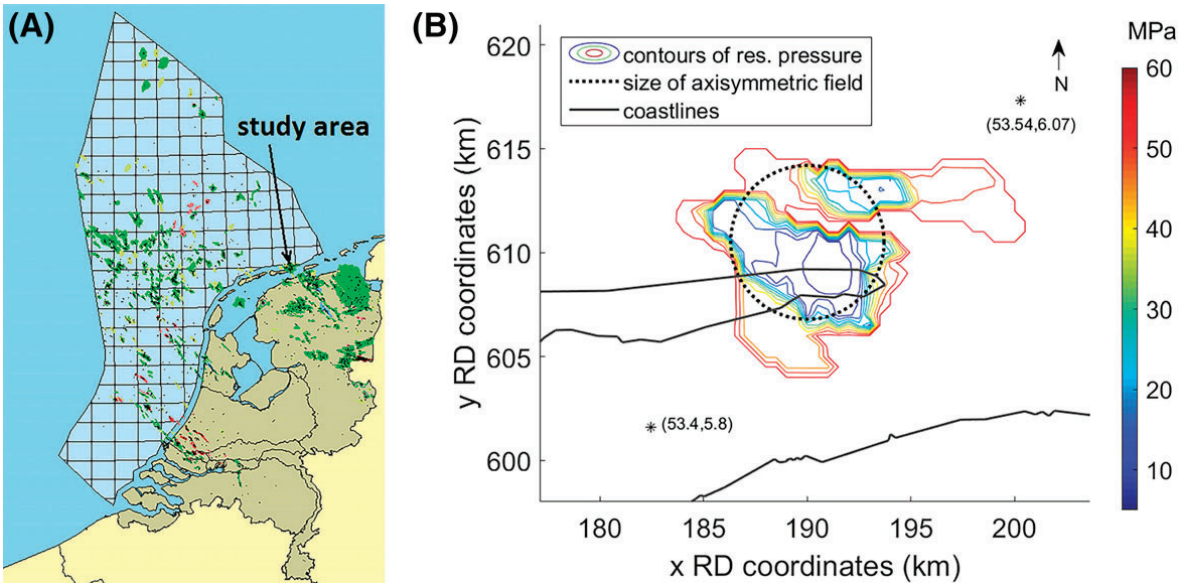

Figure 1. (A) Map of the Netherlands gas fields (green) and oil fields (red) (modified from https://www.nlog.nl/). (B) A zoom-in on the study area, including a contour plot of the reservoir (res.) pore pressure at a specific time, as supplied by the field operator, NAM. The outer contours here indicate the horizontal spatial extent of the reservoir, as well as its northern and southern lobes or compartments. Coastlines are plotted using thin black lines. The black circle represents the idealized areal extent of the gas reservoir used in the axisymmetric analyses detailed in later sections. Points indicated with asterisks (*) plot the latitude and longitude in global coordinates so as to help the reader transform Rijksdriehoeksmeting (RD) coordinates to global coordinates and locate the area of the current study.

region marked by the bold black circle in Figure 1B decreased from 56 to 26 MPa. Both the average reservoir pressure change and minimum reservoir pressure change follow a qualitatively similar trend of decreasing pressure depletion rate with time.

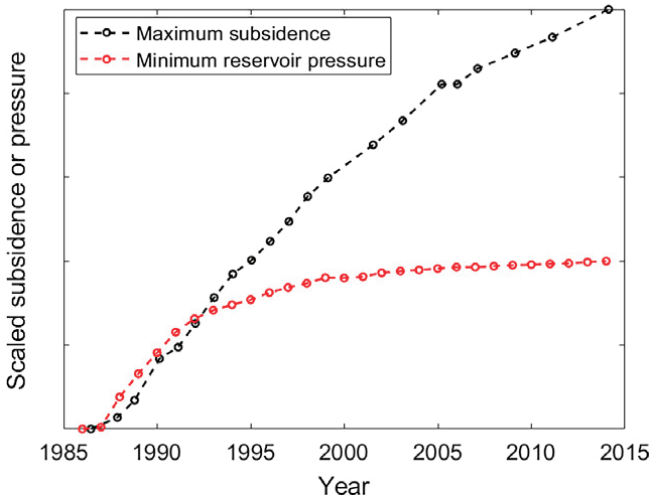

Figure 2. The time evolution of the minimum reservoir pressure (supplied courtesy of NAM) and the maximum subsidence observed over the reservoir studied. For context, the amount of measured maximum subsidence is approximately 100 mm at the point where maximum subsidence and minimum reservoir pressure signals deviate from being linearly related (approximately 1993).

Subsidence Data

Surface subsidence measurements began in 1986. The data originate from leveling campaigns performed at approximately yearly intervals between 1986 and 2014 that surveyed the same benchmarks (publicly available at https://www.nlog.nl/). Since 2006, continuous GPS data have also been available for a smaller number of locations (also available at https://www.nlog.nl/).

Figure 5 shows the spatial distribution of leveling benchmarks for which usable data are available. These are arranged along two approximately straight lines, spaced 1–2 km apart. The leveling data consist of vertical displacement relative to a benchmark remote from the field (the black asterisk in Figure 5). The reference benchmark is situated 10.6 km away from the main producing well (the black × in Figure 5), which corresponds to a distance of 9.8 km from the benchmark that registered the greatest subsidence. The 2-D axisymmetric geomechanical analyses indicate that at a distance of approximately 10 km away from the center of the field, the elastic subsidence is very small (approximately 2% of the maximum elastic, time-independent subsidence, or at maximum of the order of 1 cm—see Figure 6). Results from 2-D axisymmetric analyses that

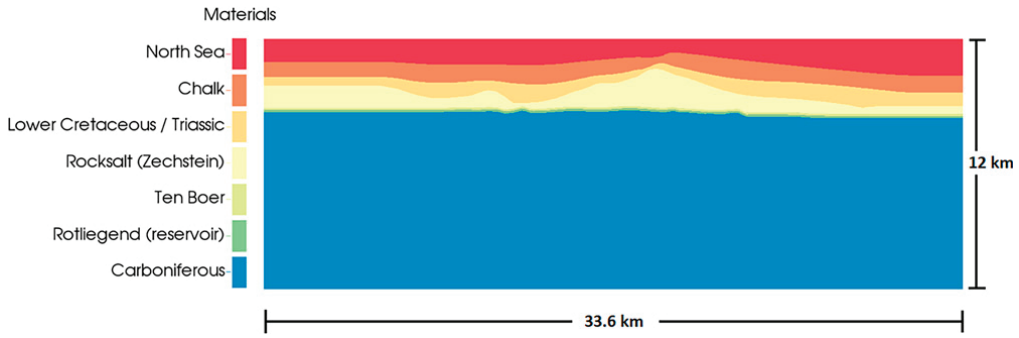

Figure 3. A west to east cross section, through the center of the three-dimensional geomechanical model for the gas field studied, showing the modeled geological succession. Note that the carboniferous does not necessarily extend to the depths shown, but has been modeled as such for lack of information and because fine material differences at depth have no significant impact on results.

include salt creep (Figure 7), and results from the 3-D geomechanical analysis (Figures 8, 9) further confirm that subsidence 10 km away from the center of the field is practically zero, confirming that the reference leveling benchmark at a distance of 10 km away from the center of the field is indeed stable.

Note that the leveling network has been extended in the most recent surveys to cover the study area's western part. These data cover only a small timespan over an area for which the subsidence signal is small. It is assumed that the leveling benchmarks were themselves stable—that is, no sinking or uplift of the benchmark relative to the ground around it. A detailed analysis of the stability of the leveling benchmarks is presented by NAM (Nederlandse Aardolie Maatschappij, 2017). A discussion on the accuracy of leveling measurements is given by Houtenbos (2011).

Figure 10 plots the total subsidence recorded along both the southern (red) and northern (blue) benchmark profiles of Figure 5, for different leveling campaigns, and shows the increase of the depth of the subsidence bowl with time. Figure 11 provides the time series for vertical displacement for three points close to the subsidence bowl's deepest point. Figure 11 also includes the vertical displacement, as measured by the continuous GPS station located at the main production well. The GPS site is 26 m from the benchmark used to plot the black curve, and the subsidence measured there agrees well with that of the leveling benchmark over the 7.5 yr for which there is data overlap. Note that the depth of the subsidence bowl in its deepest point (i.e., the maximum subsidence), which is essentially what is plotted in Figure 11, is an important quantity that will be used extensively below for comparison of model results and field data.

Figure 2, which compares subsidence to reservoir pore pressure decrease, clearly demonstrates that these are not proportional to each other, in the manner expected for a reservoir material characterized by linear elastic stress-strain behavior. This means that geomechanical model analyses are needed to examine whether the source of this anomalous time-dependence of subsidence lies in time-dependent salt flow or whether other effects such as a more complex temporal or spatial pore pressure evolution play any role. The latter are beyond the scope of this study.

MODELING THE GAS FIELD STUDIED

Modeling Method and Assumptions

The finite element method code GTECTON (Govers and Wortel, 1993, 2005) is used to perform the geomechanical analyses described herein. As will

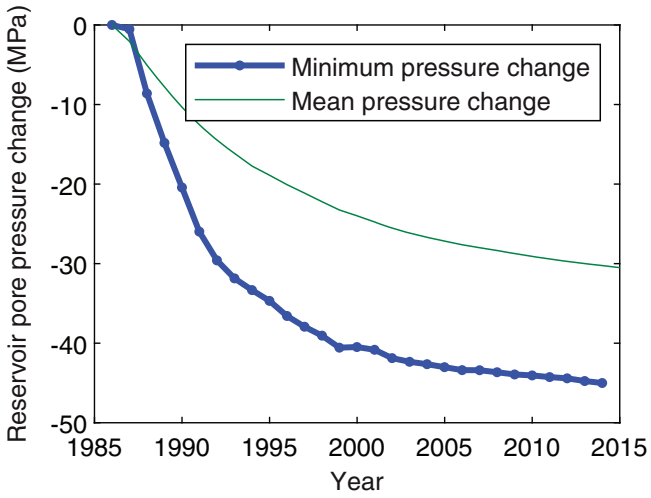

Figure 4. The evolution of the change in minimum and mean reservoir pore pressure. The change in minimum reservoir pressure forms the input to the axisymmetric geomechanical analyses.

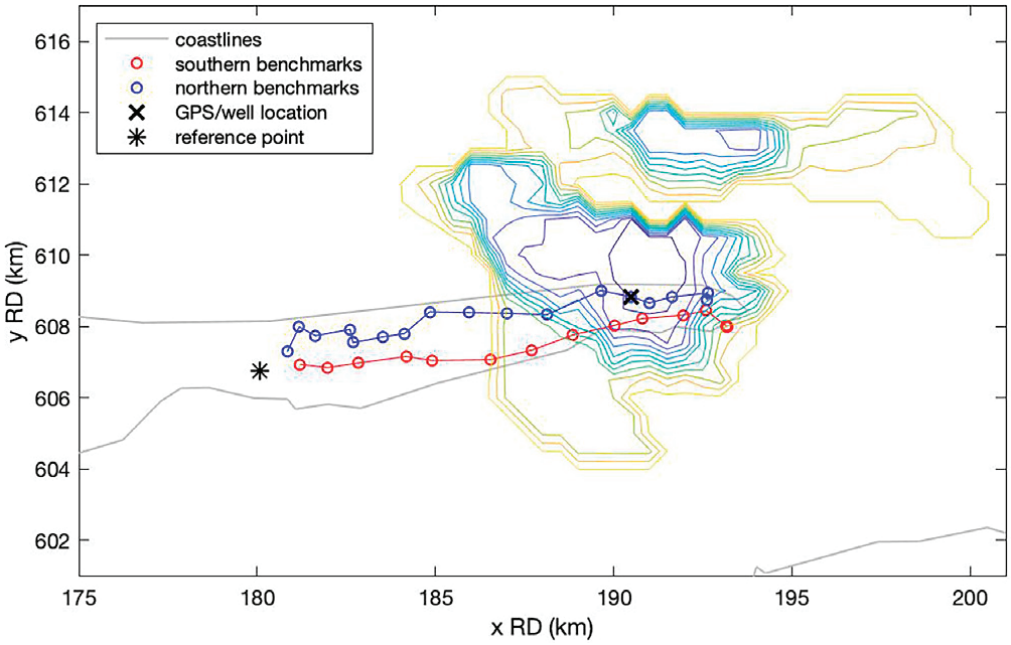

Figure 5. Locations of the leveling benchmarks used in this study. The black × marks the producing well location and the location of the continuous GPS site (data for which are shown in Figure 10). The reservoir pore pressure contours of Figure 1B are also included–these indicate the approximate extent of the producing reservoir zones. RD = Rijksdriehoeksmeting, the national coordinates system of the Netherlands.

be discussed in more detail below, here, we avoid modeling the fully coupled elastic deformation—fluid flow problem, which is only really relevant to the reservoir sandstone material. Instead, reservoir compaction that is proportional to the pore pressure drawdown is induced in the models, and this drives

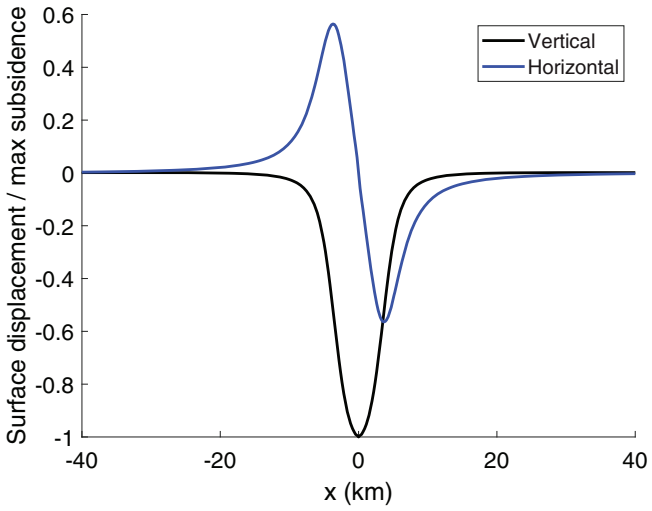

Figure 6. Axisymmetric model results assuming a fully elastic response of all rock units. The vertical and horizontal ground surface displacements plotted occur immediately upon the application of a reservoir pore pressure decrease. Both are normalized with respect to the maximum (max) vertical subsidence value. Sign convention is negative–vertical displacement signifies downward movement, and positive horizontal movement signifies movement to the right (the positive x-axis).

the elastic and creep deformation of the salt and other surrounding layers, which are assumed hydrologically shielded from the reservoir.

The GTECTON code has been validated and verified against a suite of analytical solutions, which include relaxation or straining of a viscoelastic body under constant stress (e.g., Gerya, 2010), and the analytical solutions of Verruijt (1996, 1998) for deformation around a contracting circular cavity in an elastic half-space. The majority of model realizations use the axisymmetric version of the code to achieve the speed and cost-effectiveness needed for a parametric study of salt creep laws, which requires a large number of simulations. A full 3-D analysis is also shown; this investigates whether inclusion of the asymmetries in the reservoir pressure change and geological architecture significantly affects the deformation patterns and time behavior observed in the axisymmetric models.

The GTECTON code solves the mechanical equilibrium equations for elastic and viscoelastic materials that link stresses (σ) and strains (ε) in a typical finite element method fashion. These can also be written in terms of stress and strain rates (for axisymmetric conditions) as

$$\dot{\varepsilon}_{rr} = \frac{1}{E}\left(\dot{\sigma}_{rr} - \nu\left(\dot{\sigma}_{zz} + \dot{\sigma}_{\theta\theta}\right)\right) + \frac{2\sigma_{rr} - \sigma_{zz} - \sigma_{\theta\theta}}{6\eta} \quad (1)$$

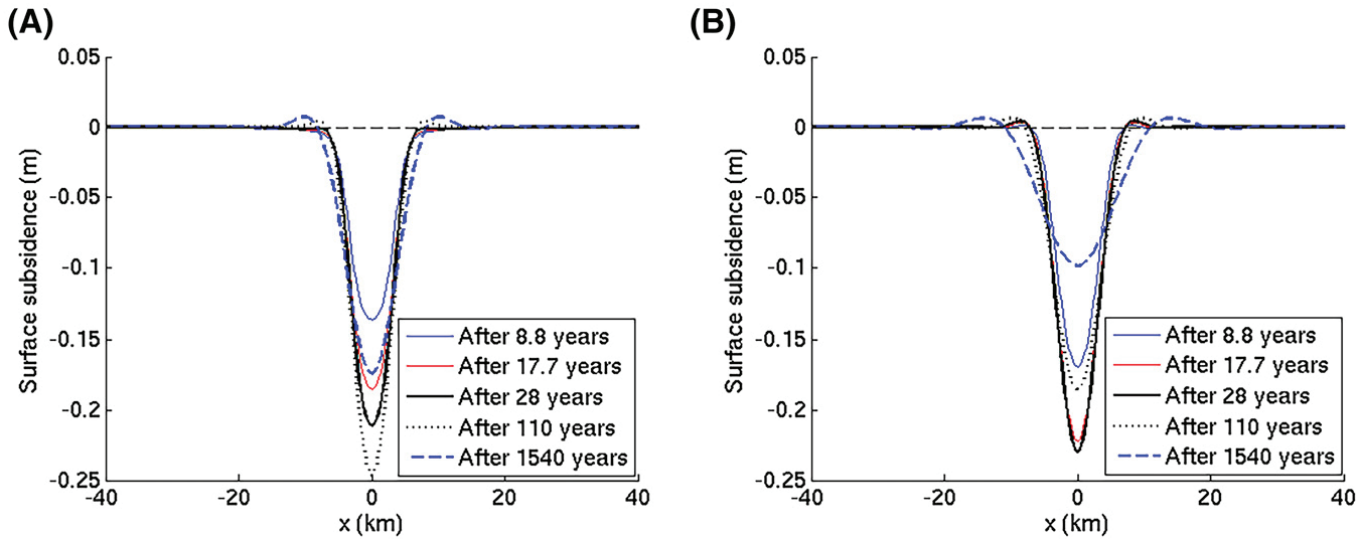

Figure 7. Axisymmetric model results for subsidence bowl development at several different times after start of production. Results from simulations that use a combined Carter et al. (1993) power-law and linear Spiers et al. (1990) flow law with a viscosity of (A) 10^{18} Pa·s corresponding to a rock salt grain size of 10.4 mm versus (B) 10^{17} Pa·s corresponding to a rock salt grain size of 4.8 mm.

$$\dot{\varepsilon}_{rz} = \frac{1+\nu}{E}\dot{\sigma}_{rz} + \frac{\sigma_{rz}}{2\eta}, \dot{\varepsilon}_{r\theta} = 0, \dot{\varepsilon}_{\theta z} = 0 \qquad (2)$$

where E, ν, and η are the material's Young's modulus, Poisson ratio, and shear viscosity, respectively (see Govers et al., 2014). A dot placed over a symbol signifies the rate of change with time, and subscripts r, z, and θ denote the radial, vertical, and tangential (i.e., horizontal into the page) directions, respectively. For nonlinear creep laws, the shear viscosity η is dependent on shear stress level. Note that for all materials modeled here, apart from salt, the viscosity is assumed infinite, viscous strain rates are accordingly zero, and the above equations revert to elasticity. Equations similar to equation 1 apply to the strain rates in the other directions ($\dot{\varepsilon}_{zz}$ and $\dot{\varepsilon}_{\theta\theta}$), whereas $\dot{\varepsilon}_{r\theta}$ and $\dot{\varepsilon}_{\theta z}$ are zero due to the assumed axisymmetric condition. For the 3-D analyses, equations for the strain rates in the xx, yy, and zz directions are similar to equation 1, and equations for the shear strain rates are similar to the equation for $\dot{\varepsilon}_{rz}$ (see Govers and Wortel, 2005). This study adopts the convention that compressive stresses and strains are positive.

No change of temperature in the geomechanical system is modeled, as there is no field evidence for such a temperature change. It is further assumed that initially (i.e., at t=0 in the analyses, and before the start of production in the in situ reservoir), the salt body is in equilibrium, and the deviatoric stresses inside it have relaxed to approximately zero. This is a reasonable assumption, as there was no reported ground subsidence or uplift in the area before the start of production. We note also that natural salt microstructures preserve subgrain size evidence that generally suggest in situ deviatoric stresses of the order of 0.1 to 1 MPa in nearby salt bodies (see e.g., Schléder and Urai, 2005).

The code used here does not model pore pressure inside a geomaterial explicitly. The effect of gas production, which leads to a pore pressure decrease in the reservoir rock, is modeled as an externally applied increase in the mean stress acting on the reservoir material, thus simulating an increase in effective mean stress. The magnitude of this applied increase in mean compressive stress at any given time is set equal to the magnitude of the reservoir pore pressure decrease, as calculated from the NAM reservoir pore pressure analysis data. This is equivalent to a value of 1 for the Biot coefficient of the reservoir material. The above scheme for the application of the reservoir pore pressure reduction is based on the Terzaghi (1943) principle of effective stress. This postulates that the total stress can be separated into the pore pressure carried by the pore fluid and the effective stress carried by the solid skeleton of a porous material. It is then the effective stress (i.e., the difference between the total stress and the pore pressure with compression positive) that causes deformation of the material's skeleton. Thus, the effective reservoir stresses can be linked to elastic

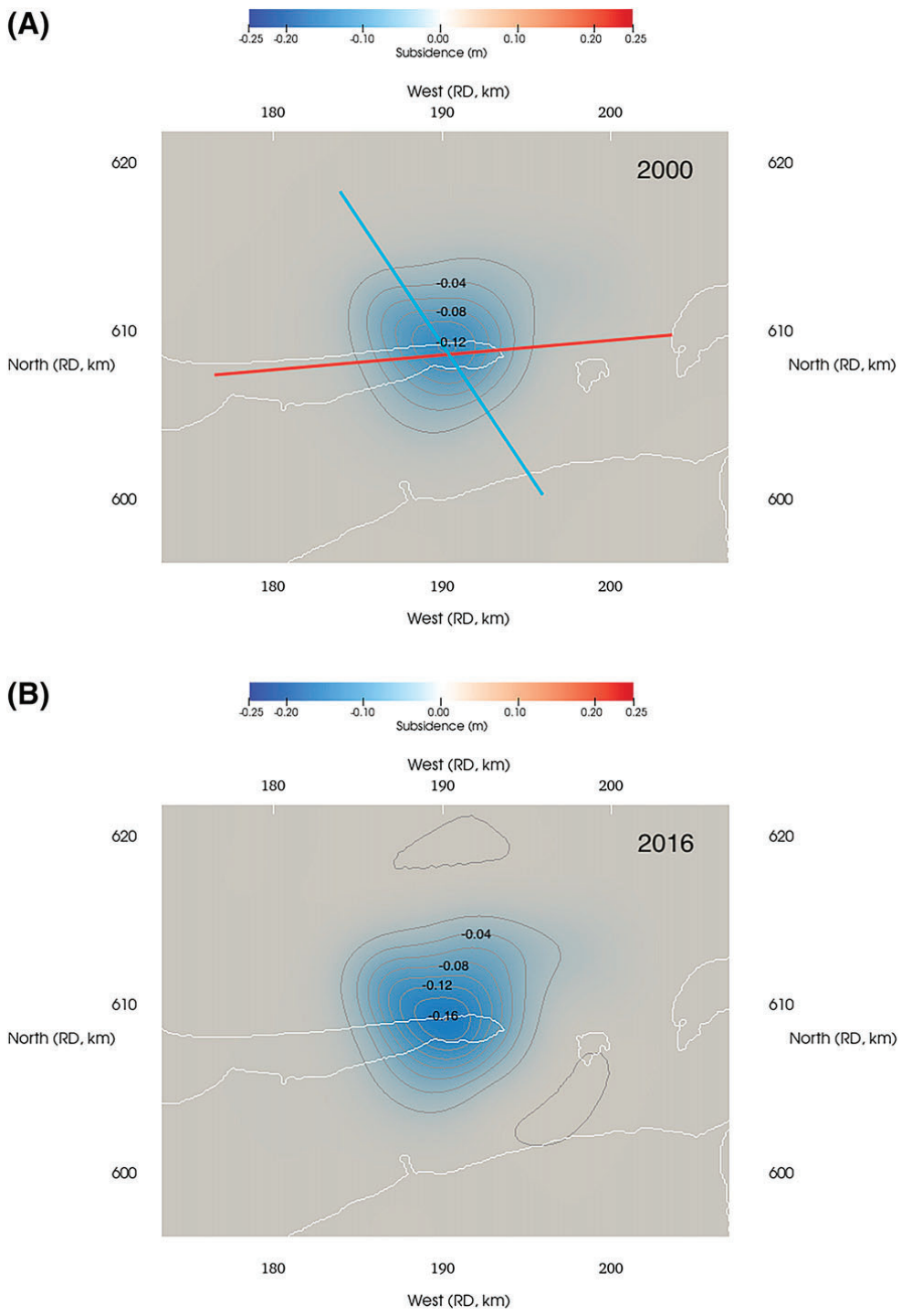

Figure 8. Three-dimensional geomechanical model results. Contours of subsidence caused by elastic deformation and linear rock salt flow, resulting from reservoir pressure reduction (A) 14 yr and (B) 30 yr after the start of gas production. RD = Rijksdriehoeksmeting, the national coordinates system of the Netherlands.

reservoir strains in the models presented here through the reservoir material's elastic parameters (i.e., through equations 1 and 2).

Usually, pore pressures need time to equilibrate inside materials of low porosity. However, here, the reservoir sandstone is assumed to be of sufficiently high porosity and permeability to presume that any pore pressure reduction at the well is more or less instantly evenly distributed across the whole of the axisymmetric model reservoir. Figure 4 shows that the change in both the average and minimum reservoir pore pressure qualitatively follow the same trend

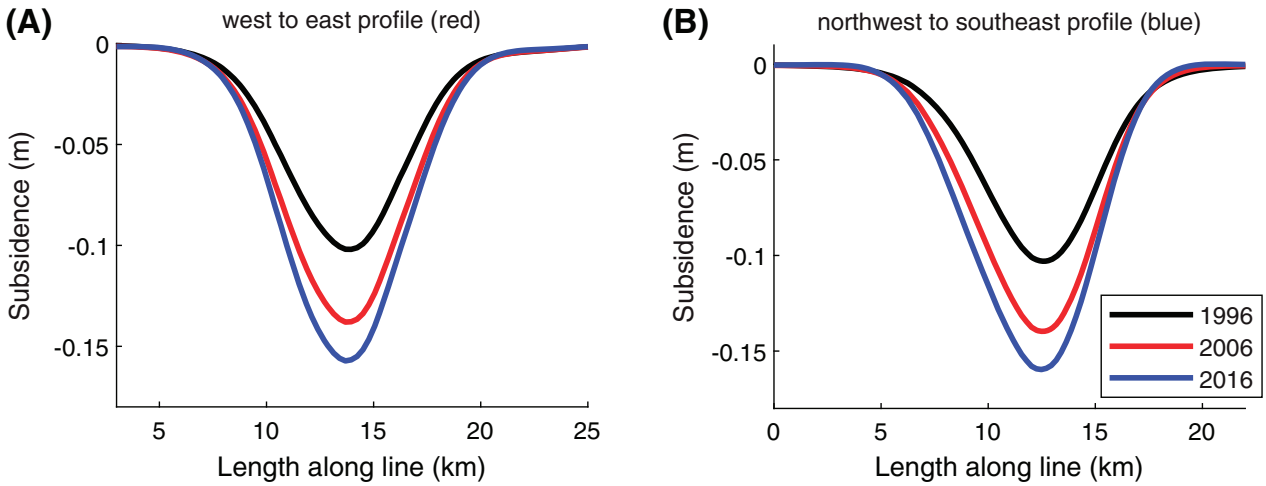

Figure 9. Three-dimensional model results for the gas field studied. Cross sections (along the lines marked in Figure 8A) illustrating the modeled subsidence bowl produced assuming elastic deformation and linear rock salt flow only. (A) West to east profile. (B) Northwest to southeast profile.

versus time. Hence, use of the minimum reservoir pressure as input to the axisymmetric analysis makes no qualitative difference to the subsidence results obtained. It only affects the magnitude of subsidence, which is also affected by choices for other parameters' values (e.g., the elastic modulus of the reservoir rock).

In reality, the pore pressure inside the reservoir rock is close to, but not entirely, uniform (Figure 5). Further, the reservoir consists of two Rotliegend sandstone units, separated by a thin intervening claystone. This fine detail is captured in the 3-D analysis, which uses a weighted average of the pressures within these two linked Rotliegend reservoir sandstone layers and applies the change in this weighted average as a compressive mean effective stress increase at each point for which pressure data are available. Therefore the 3-D model more accurately represents the spatial distribution of reservoir pore pressures and further captures the fact that a smaller satellite field northeast of the main reservoir (see Figure 5) started production with a delay of approximately 8 yr.

In this paper, wherever future subsidence evolution is shown, the authors artificially assume that gas production stopped in 2014 and that reservoir pore pressure remained constant thereafter—in other words,

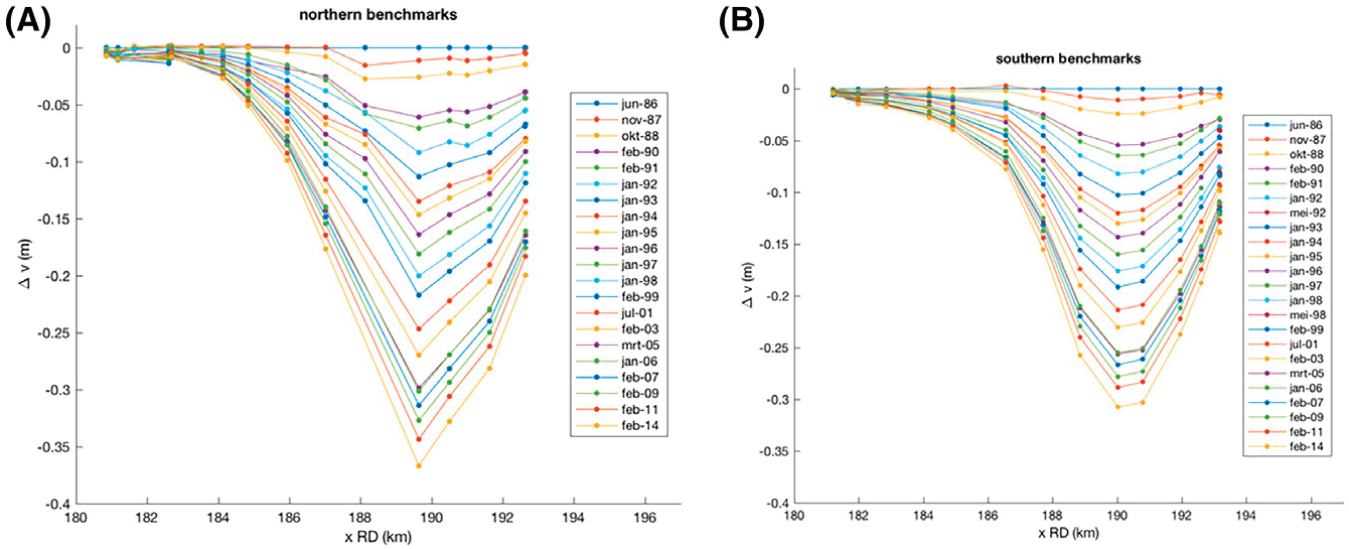

Figure 10. Time evolution of vertical displacement of benchmarks lying along (A) the northern and (B) the southern leveling traverses acquired for the field studied. The curves approximately represent cross sections of the observed subsidence bowl (for locations of the benchmarks and traverses, see Figure 5). RD = Rijksdriehoeksmeting, the national coordinates system of the Netherlands.

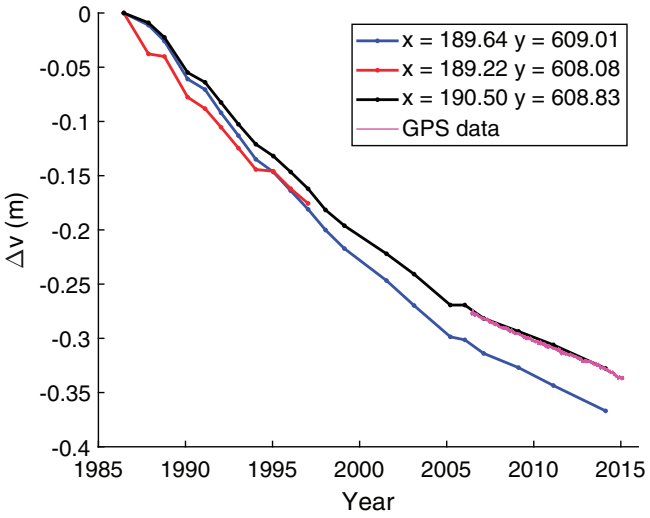

Figure 11. The evolution of vertical displacement as measured at the leveling benchmarks registering maximum subsidence (red and blue curves) and at the benchmark located closest to the production location (black curve). The vertical motion of the production site as measured by GPS is shown in pink. Data are provided by NAM and publicly available via https://www.nlog.nl/; curves are labeled according to the x and y coordinates of the benchmarks. We only present data up to 2014 as the newest data did not form part of this geomechanical study. Note, however, that data publicly available at https://www.nlog.nl/ indicate that the benchmarks represented by the blue and black curves registered an additional 15.7 and 12.7 mm of subsidence respectively, between February 2014 and January 2017.

that the reservoir was fully sealed from its surroundings and any ongoing changes with time beyond 2014 were caused by salt flow.

Material Behavior and Modeling Salt Creep

This study assumes that all rock materials are homogeneous and isotropic. All materials are modeled as linear elastic except for the salt, which is modeled as a viscoelastic Maxwell material, meaning that an element of salt can be visualized as a spring in series with a dashpot in the shear direction. Salt creep behavior is described in detail by Marketos et al. (2016), where the grain-scale mechanisms responsible for creep are also discussed. Here, we focus on modeling steady-state creep and approximate transient creep behavior by using a reduced salt elastic modulus, as was done by Prij (1991) and Marketos et al. (2016). We use several models for salt flow that have been proposed in the literature (Munson and Dawson, 1979; Spiers et al., 1990; Carter et al., 1993; Hunsche and Hampel, 1999; Figure 12; Table 1) whereby the steady-state creep strain rate at a given shear stress can be calculated through the following equation:

$$\dot{\varepsilon}_{axial} = Ae^{-Q/RT}\Delta\sigma^{n} \quad (3)$$

Here, A is a constant, Q is the (apparent) activation energy for the micromechanism that is responsible for creep (in J/mol), R is the universal gas constant (8.314 J/mol/K), T is the temperature in Kelvin, n is a dimensionless stress exponent, and $\Delta\sigma$ is the difference between applied axial and radial stress in a triaxial creep experiment. Note that the temperature here has been taken as 100°C (373 K), which is the temperature of the same evaporite unit elsewhere in the Netherlands, at approximately the same depth (e.g., Breunese et al., 2003). Equation 3 relates the axial strain rate to the principal stress difference in a triaxial test but can be converted to shear strain rate versus shear stress to obtain viscosity.

The most important creep micromechanisms in salt are dislocation creep (e.g., Carter et al., 1993; Hunsche and Hampel, 1999) and fluid-assisted

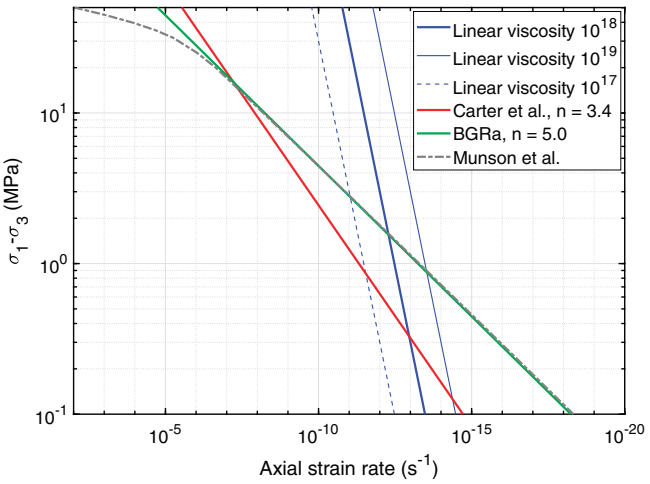

Figure 12. The predictions for principal stress difference in a triaxial compression creep test plotted against axial strain rate for commonly used steady-state flow laws for rock salt, plotted here for a temperature of 100°C, which is close to the temperature of the reservoir studied. Linear viscosities of 10^{17}, 10^{18}, and 10^{19} Pa·s correspond to pressure solution creep in salt with grain sizes of 4.8, 10.4, and 22.4 mm, respectively. Note that in the case of a combined, two-mechanism creep flow law, the easiest (weakest) mechanism is expected to dominate at a given strain rate and that the x axis has been reversed. The flow laws used in the present study are listed in Table 1. The Munson et al. flow law, developed by Munson and coworkers over the years, is given in Munson and Dawson (1979) and the creep flow law BGRa is given in Hunsche and Hampel (1999).

Table 1. The Parameters for the Halite Salt Creep Laws Used Here (See Equation 3)

Flow Law	n	A, $MPa^{-n}s^{-1}$	Q, kJ/mol
Carter et al. (1993)	3.4 ± 0.1	$8.1 \times 10^{-5} \pm 2.7 \times 10^{-5}$	51.6 ± 1.2
Spiers et al. (1990)	1.0	$(3.76 \times 10^{-13} \pm 1.89 \times 10^{-13})/T/D^3$ effective grain size (D) and temperature (T) dependent	24.5 mean value
Hunsche and Hampel (1999) (BGRa)	5.0 mean value	2.1×10^{-6} mean value	54 mean value

diffusion creep or pressure solution (Spiers et al., 1990); see Table 1. Each creep mechanism active at the grain-scale is linked to a specific creep equation with its own set of A, Q, and n values. As some of these micromechanisms can be active in parallel inside the material (i.e., as parallel-concurrent microscale transport processes driven by the same stress difference, and hence as serial elements in mechanical analogue representation), the total strain rate can be calculated as the sum of the strain rates for each micromechanism. The constant A is inversely proportional to the cube of the grain size of salt for linear (pressure solution) creep (n = 1), whereas it is grain size-independent for power law (dislocation controlled) creep (n = 3–5 typically). The relevance of the salt creep laws mentioned herein to the present gas field will be further discussed in the Results section, where also uncertainties in the creep laws themselves and their input parameters will be discussed.

The Geological Model

The geology of the field studied—that is, the reservoir system and surrounding lithological formations—is complex from a modeling perspective. Although the sedimentary sequence is near-horizontal, it includes faults, thickness variations in the various units, secondary variations and inhomogeneities within each unit itself, and a complex 3-D reservoir shape.

Many of the above complexities, including the presence of faults, are ignored in the axisymmetric model, which is used to test the sensitivity of the results to the choice of salt creep law. In the axisymmetric model, the different lithological units are set to be horizontal. The extent and material properties of each formation are given in Table 2. The Rotliegend sandstone unit extends to the axisymmetric domain's edges (i.e., to the rigid vertical frictionless boundaries that were placed at a radius of 55.8 km, i.e., sufficiently far from the reservoir, at locations where salt flow will be zero). Still, only part of it is assigned to the reservoir. The reservoir is idealized as a disk 100 m thick (the approximate thickness of the reservoir sandstone layer) and diameter 7.5 km (see Figure 1B for an overlay on a plan view of the pore pressure contours, which themselves delineate the gas field), having rounded edges with a radius of curvature of 50 m. This radius of curvature is chosen so as to maintain consistency with previous models (e.g., Marketos et al., 2015b). Variations in this choice induce only very local effects on the stress distribution within the model and have no significant impact on subsidence results. Similarly, small changes in the equivalent axisymmetric reservoir diameter have little effect on the calculated subsidence patterns.

The 3-D analysis is based on the 3-D geomechanical model supplied to us by NAM (see Figure 3) and replicates it as closely as possible. The extent of the 3-D geomechanical model is 33.6 by 25.6 km wide and 12 km deep. In the 3-D analysis, the effect of nonuniform salt top seal thickness is included (this varies from 60 to 2300 m in the area of interest). The NAM geological model was modified by increasing the minimum thickness of the salt and Ten Boer claystone layers to 200 and 100 m, respectively (to avoid very small elements; these were originally present close to the geomechanical model edges). Discrete faults are ignored, including their offset in the geological layering, in the few cases where this is significant (Figure 3). Finally, the 3-D model uses the same material properties as for the axisymmetric analyses (Table 2), apart from the salt, for which a linear viscoelastic material with a viscosity of 10^{18} Pa·s is used. This is instead of investigating the full range of proposed salt creep laws or using a composite flow law, such as a combined Carter

Table 2. Material Properties and Depths of the Geological Units Used in the Simulations

Unit Name	Young's Modulus, GPa	Poisson Ratio	Depth Range for the Unit (m)—Axisymmetric Model
North Sea	2	0.30	0–850
Chalk	10	0.25	850–1600
Lower Cretaceous/Triassic	16	0.25	1600–2000
Rock salt (Zechstein)	30—viscoelastic (see Table 1)	0.35	2000–3250
Ten Boer claystone	40	0.20	3250–3350
Rotliegend sandstone (reservoir)	20	0.20	3350–3450
Carboniferous shales/siltstones	40	0.20	3450–39,600

Depths apply for the axisymmetric simulations and are only approximate for the three-dimensional (3-D) analyses, as geological layers in 3-D analyses are not uniform in thickness. Material properties are after Mossop et al. (2011), with the exception of the modulus for the reservoir sandstone, for which we select a value within the range given by these authors. Note that the deepest layer modeled (carboniferous) is extended to the base of the model; modeling accurately the geological sublayering below a certain level is not necessary, and furthermore, not much information is available on the underlying layers.

et al. (1993) dislocation creep law plus linear salt creep law.

RESULTS

As mentioned above, most simulations conducted here are axisymmetric (pseudo-3-D), allowing the effects of different salt creep laws on subsidence to be investigated in an efficient way through the use of an idealized geomechanical model. The 3-D analysis conducted (which uses a purely linear salt creep law) complements the axisymmetric analyses by removing some of these constraints. It allows a full investigation of the effects of the asymmetry seen in the field geometry (Figures 1B, 3) and of the spatial-temporal evolution of the reservoir pore pressure, both of which it addresses as accurately as possible.

Axisymmetric Model Results

Elastic (Time-Independent) Response to Reservoir Pore Pressure Decrease

Upon reducing the reservoir pore pressure, the model reservoir compacts elastically, and the surface subsides in a manner determined by the pore pressure change only. In reality, some of the reservoir compaction will be inelastic—that is, irrecoverable (Pijnenburg et al., 2018, 2019). However, here, we use the approximation of linear elasticity for the reservoir rock and surrounding materials, then introducing salt creep mechanisms to examine their impact on subsidence evolution. Figure 6 plots both horizontal and vertical elastic displacements caused by unit reservoir (pore) pressure reduction. These displacements are plotted against radial distance from the model's center and normalized with respect to the maximum vertical displacement value. Note that for a linear elastic reservoir material, the immediate (elastic) response to any pore pressure reduction can be calculated by multiplying the curves of Figure 6 by the ratio of the pore pressure reduction values to the normalizing unit value.

How Salt Cap Rock Creep Generates Ground Surface Movements

In all the models, variations in subsidence with time are the result of both a gradual reduction in reservoir pore pressure due to gas extraction (i.e., to a time-varying forcing) and of salt creep. The way in which gas extraction translates to subsidence through salt creep is as follows: A reservoir pore pressure reduction leads to a mean effective compressive stress increase inside the reservoir rock, which in turn induces volumetric strains, reservoir compaction, and changes in stress and strain in the surrounding material layers. This results in the development of significant shear stresses, particularly around the edges of the reservoir (see Figure 13A) and inside the salt top seal.

As salt is a material that flows (creeps) to relax shear stresses developed inside it, time-dependent displacements occur (in addition to the elastic displacements) until the shear stresses in the salt have fallen to a sufficiently low value—to zero in Figure 13B. This figure also shows the corresponding normalized displacement field induced by salt creep

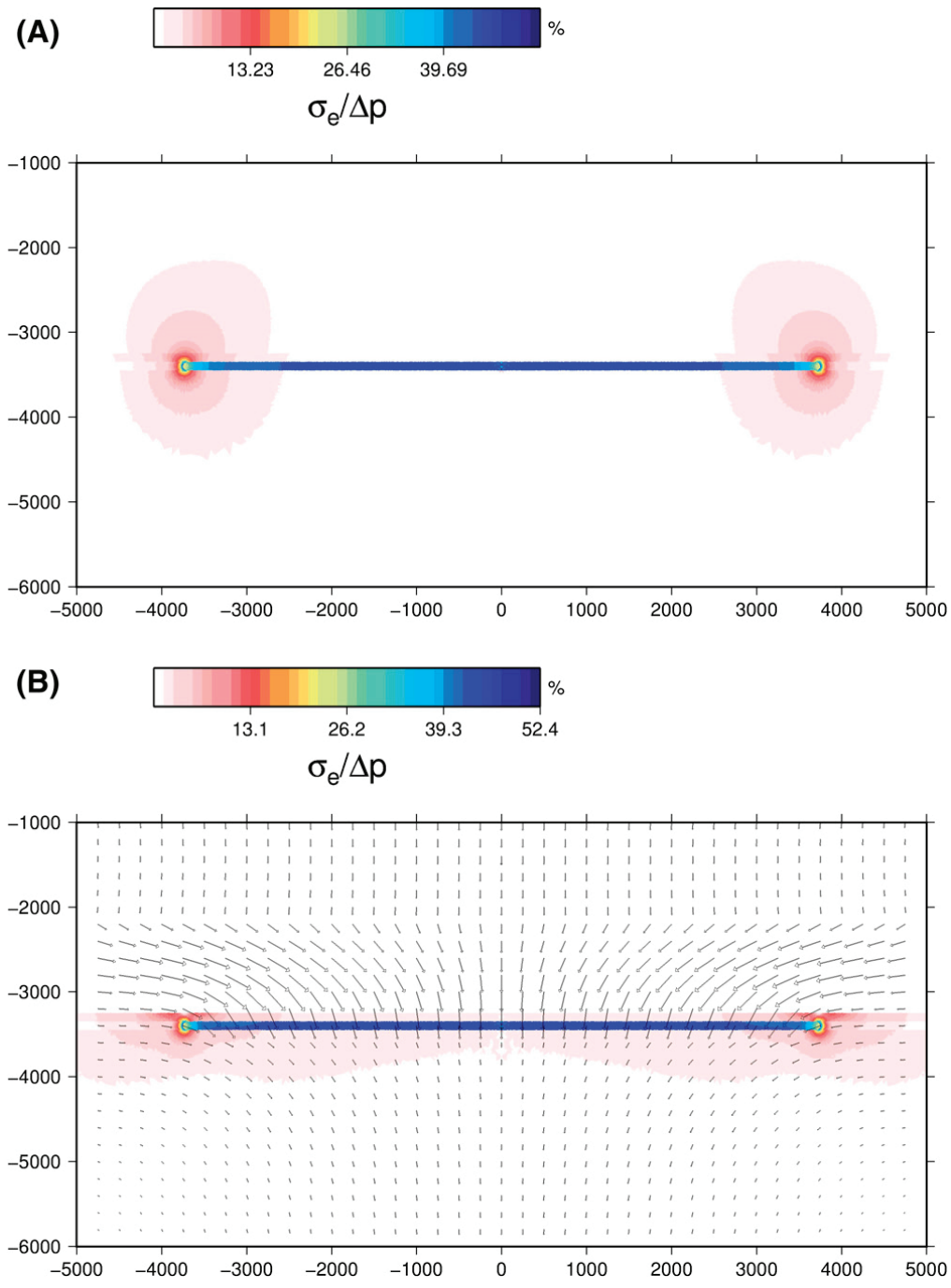

Figure 13. The square root of the second invariant of the deviatoric stress tensor (σ_e, a measure of shear stress) in the axisymmetric reservoir model is plotted here as a percentage of a fixed reduction in reservoir pore pressure (Δp) that is applied at time equals zero (A) immediately after the pore pressure reduction (the elastic solution) and (B) after sufficient time has passed so that the shear stresses of (A) inside the rock salt layer (extending from $z = -2000$ to -3250 m) have fully relaxed by creep assuming a linear rock salt creep law. (B) also plots the accumulated displacement field after full rock salt relaxation (displacements again proportional to Δp).

after an initial step reduction in reservoir pore pressure. Note that Figure 13B shows results from a fully linear geomechanical model—that is, one that assumes the same linear salt creep equation as used in some of the authors' previous work (e.g., Marketos et al., 2016). Results obtained using the more complex and more realistic salt creep models applied herein would be very similar.

It is worth remarking here that there is merit in calculating the step response for linear salt creep

(especially if this approximates creep in the field). This is because, in this special case, the modeled geomechanical system is linear (provided the reservoir material remains linear too), so that the principles of superposition, and of convolution of a "system step response" (i.e., the subsidence response to a unit reservoir pore pressure decrease) with the reservoir pore pressure reduction history (i.e., the input excitation), can be used to quickly build subsidence evolution solutions. Marketos et al. (2015a) show that the response to a step decrease in reservoir pore pressure is an initial deepening of the subsidence bowl, followed by volume redistribution and shallowing at larger times.

The Effect of Salt Creep Uncertainties on Subsidence Evolution: Results from the Axisymmetric Geomechanical Model

There is large uncertainty with respect to the rheological model that best describes salt creep, especially at low stresses (see Marketos et al., 2016 for a more extensive description) as demonstrated by the large number of models that have been proposed (see Table 1 for common salt creep laws). This uncertainty is partly due to the lack of long-term experimental data and partly due to the fact that the creep behavior is highly grain size sensitive (Table 1), whereas the grain size of natural salt at a specific site is often poorly constrained.

Some published salt creep laws are thought to be more relevant than others, depending on the salt water content or grain size. For example, a one-component power law with an exponent of 5 (e.g., BGRa, the creep flow law given in Hunsche and Hampel [1999], or Munson and Dawson, 1979) is thought to represent a dislocation-controlled microprocess that may dominate in dry halite. This may also dominate in halite where fluid-assisted processes active at fluid-filled grain boundaries, such as pressure solution or grain boundary migration, are inhibited due to (1) large grain size, (2) the formation of isolated fluid inclusions at low stresses due to surface energy reduction (see van Noort et al., 2008), or (3) grain boundary microcracking and fluid film disruption at low confining stresses (Urai et al., 2008). Natural salt almost always contains more than a few parts per million of water, and the confining stresses present at the depth and temperature conditions relevant to top seals of reservoirs similar to the one studied here are sufficient to suppress dilatancy, allowing fluid-assisted effects to develop and control creep flow rates. The Carter et al. (1993) flow law was obtained in unusually long-term tests under zero dilatancy conditions and at pressure and temperature conditions that are relevant to the gas field considered here. The authors therefore consider the Carter et al. (1993) power law, combined with the linear Spiers et al. (1990) flow law for "pressure solution" to be the most representative of natural salt behavior. In the axisymmetric models, we apply these combined flow laws for salt with grain sizes of 4.8, 10.4, and 22.4 mm (note: in the linear "pressure solution" creep law, viscosity is grainsize-dependent [see Table 1], and these grainsizes yield linear shear viscosities of 10^{17}, 10^{18}, and 10^{19} Pa·s, respectively). These grain sizes are within the range (3–20 mm) reported by Breunese et al. (2003) for nearby salt at the same stratigraphic level as modeled here.

Figure 7 shows the cross section of the resultant surface subsidence bowl at a number of different times in response to the reservoir pore pressure decrease shown in Figure 4 (see section above on modeling for more details) for salt flow governed by the combined Carter (power law) and linear pressure solution models. The bold continuous black curve represents the subsidence bowl at the end of production in the models (the year 2014, i.e., 28 yr after the start of production). Figure 7A shows subsidence for a salt grain size of 10.4 mm, whereas Figure 7B shows results for a grain size of 4.8 mm (i.e., linear shear viscosities of 10^{18} and 10^{17} Pa·s, respectively, for the pressure solution part of the combined creep mechanisms used).

In both Figure 7A, B, the subsidence bowl deepens initially as the pore pressure falls due to gas extraction, and the reservoir compacts. However, even before the end of gas production (at 28 yr in the model), the subsidence bowl is different for the two different salt creep models (i.e., for the two different salt grain sizes). This behavior can be explained by thinking of the response to a step change of reservoir pore pressure; initially, a step pore pressure decrease leads to a deepening of the subsidence bowl, followed by a shallowing as the subsidence volume redistributes at much larger times, and the times at which the switch from deepening to shallowing occurs is proportional to the speed with which salt creeps (see Marketos et al., 2015a). Salt flow is faster for the finer-grained salt material (Figure 7B), so the

subsidence bowl at the end of production (28 yr) is deeper. In Figure 7A, as the salt is coarser and so creeps slower, the salt has less time to relax in the 28 yr of gas production, and the subsidence bowl continues deepening, even after the modeled end of production. By contrast, for the finer grain size (faster salt creep), no further deepening of the subsidence bowl occurs after gas production ends in the model (28 yr). This could be a significant observation in the context of the field studied, as 28 yr corresponds to the year 2014, the last point for which the subsidence data are analyzed. Better characterization of the salt grain size, which controls linear salt material element creep timescales, could therefore help predict whether maximum salt-induced subsidence might continue growing in the field in the future. Note, however, that other mechanisms could cause additional subsidence (e.g., reservoir creep or poroelastic deformation due to pore pressure equilibration in the system)—see Nederlandse Aardolie Maatschappij (2017), which documents an investigation into other mechanisms, and Fokker et al. (2018).

For both results shown in Figure 7, significant redistribution of subsidence bowl volume occurs as the subsidence bowl becomes shallower and wider at large times beyond the end of production. This subsidence rebound is caused by movement of salt toward the region overlying the center of the reservoir, which occurs because the pressure solution mechanism (i.e., linear salt creep) is assumed to continue until full relaxation of shear stresses is achieved in the salt. However, it is not certain whether this rebound will actually take place, and the authors are not aware of any field situation where such a reversal of vertical deformation has been firmly observed to date. It is possible, for example, that the low stress behavior of salt, which is only constrained experimentally for synthetically prepared, fine-grained salt (with the recent notable exception of the experimental study by Bérest et al., 2019), actually follows a different flow law, due to different microstructures, water, and impurities content, for example. This point will now be explored through discussion of results for different salt flow laws.

Figure 14 plots the time evolution of the vertical displacement of the deepest point of the subsidence bowl (the ground surface point above the center of the reservoir). It includes the result for a fully linear elastic system (i.e., noncreeping salt and linear elastic

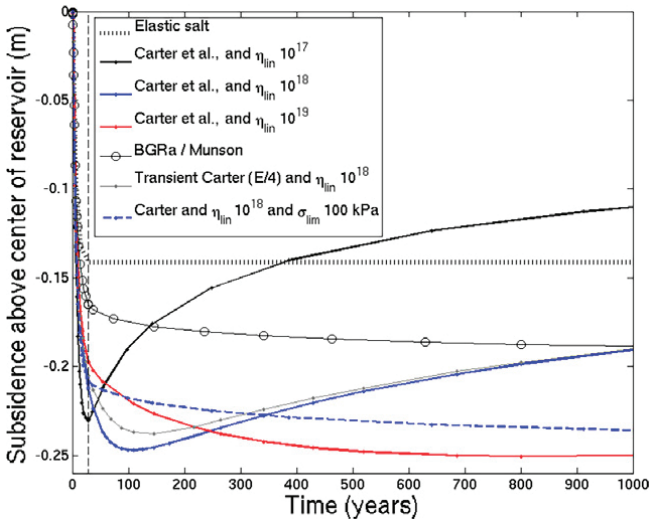

Figure 14. The time evolution of vertical displacement at the deepest point of the subsidence bowl—that is, at the ground surface point above the center of the reservoir, as obtained in axisymmetric simulations in which only the constitutive model for rock salt was varied. Time is measured since the onset of production. The creep flow law BGRa is given in Hunsche and Hampel (1999).

reservoir material) for purposes of comparison and shows that salt creep for this reservoir size leads to a measurable effect—as much as 75% of the maximum subsidence produced by the fully linear and elastic model (i.e., at the deepest point of the subsidence bowl). In practice, predictions of future subsidence are usually made by calibrating models to measured subsidence, meaning that the linear (elastic) models used by industry already account for much of this effect of salt creep (which occurs during production) through a back-calculated, calibrated increase in elastic compressibility of the reservoir material. This was not done here, as the purpose was not to predict future subsidence but to create a forward model for assessing the relevance of salt creep in causing the anomalous time-dependence of subsidence observed over the gas field.

Figure 14 also includes the maximum subsidence evolution for a number of different creep laws for salt. It thus aids visualization of the effect of uncertainties in salt creep law on the subsidence response. For example, it includes results for the most plausible combined Carter et al. (1993) plus Spiers et al. (1990) flow law for salt grain sizes of 4.8, 10.4, and 22.4 mm that are relevant to the gas field studied. It also includes results for a one-mechanism (dislocation creep) power law with an exponent of 5

(e.g., BGRa or Munson and Dawson, 1979), which is commonly used, but which is thought to be less appropriate (see above).

Figure 14 includes results for a combined linear and power law creep model in which the linear creep mechanism is deactivated below a specific stress limit (here 100 kPa). This macroscale stress limit is theoretically justified by assuming a grain boundary healing microprocess, in which the thin water films that support pressure solution creep (i.e., allow material diffusion from grain contacts under high normal stress to those less highly stressed) become disconnected (see van Noort et al., 2008), thereby inhibiting linear creep. Once again, though, this healing behavior and the associated several-orders-of-magnitude decrease of salt strain rates has not been observed experimentally, and, therefore, uncertainties in quantifying this process mean that the value for the macroscale stress limit can lie anywhere in the range of 0.1 to a few megapascals, according to the model presented by van Noort et al. (2008) when applied for NaCl (see also Desbois et al., 2012 which discusses this effect). Note also that Bérest et al. (2019) report recent long-term creep experiments in which salt creep is observed at stresses as low as 0.2 MPa, further constraining the stresses below which the above-mentioned healing micromechanism might inhibit creep for the particular salt they tested.

Figure 14 also briefly covers the topic of transient creep. Transient creep is approximated by reducing the salt elastic moduli (here by a factor of 4), as also done by Prij (1991), for example. This is more fully discussed by Marketos et al. (2016).

Figure 14 shows that the uncertainties in the salt creep law considered lead to uncertainty in the subsidence response both in terms of maximum subsidence and also in terms of the timescale over which this evolves. For example, the use of some creep laws leads to ongoing deepening of the subsidence bowl after cessation of production (marked by a vertical black broken line in Figure 14). Similarly, subsidence rebound is observed only for some choices of flow law.

Note that the salt creep process investigated here is a constant volume process, so it does not increase subsidence volumes (i.e., the volume of the subsidence bowl) but merely redistributes subsidence volume from one area to another once the driver for subsidence (i.e., gas extraction) stops. This is potentially significant; van Thienen-Visser et al. (2015) focus on subsidence volumes, and not maximum subsidence, as the most appropriate subsidence impact indicator for the shallow coastal basins of the Netherlands.

3-D Model Results

For the 3-D modeling, the salt is set to a linear viscoelastic material with a viscosity of 10^{18} Pa·s, which corresponds to the authors' best estimate of the salt's linear viscosity based on what is known about the grain size of similar salt bodies in the field's vicinity. Even though a combined Carter et al. (1993) and linear salt creep law in 3-D analyses is more realistic, a material with a constant viscosity is expected to lead to very similar 3-D subsidence results for the limited ranges of deviatoric stress observed in the model. This is because the transition between linear and power law creep would, in this case, occur at more than 0.3 MPa (Figure 12), meaning that the bulk of the salt volume would, in any case, creep through a linear creep law. Marketos et al. (2016) show that results for a linear creep and a combined Carter et al. (1993) and linear creep law with a viscosity of 10^{18} Pa·s are almost identical for axisymmetric simulations for a similar-sized field, confirming the point above.

Figure 8 shows the 3-D model subsidence contours for two moments in time: 14 and 30 yr after beginning of production (corresponding to the years 2000 and 2016). Both contour plots show that the subsidence pattern is asymmetric: the modeled subsidence bowl is generally deeper in the north and extends to the northeast, too.

Figure 9 shows the model results obtained for the subsidence bowl in west to east and northwest to southeast sections across the field—refer to Figure 8A for section location. Note that these sections do not necessarily pass through the deepest point of the 3-D modeled results. The subsidence pattern changes little in shape but migrates to the northwest in later years (Figure 8). When the authors examined the location of the deepest point in the 3-D simulation, they found this to be relatively stable and insensitive to asymmetry of the thickness of the salt layer (Figure 3) and changes in location of production.

COMPARISON OF MODELED VS. FIELD SUBSIDENCE

Figure 15 compares the leveling data for one of the benchmarks situated above the middle of the field to the geomechanical model results. As all three time series in the leveling data of Figure 11 are similar, the choice has been made to plot the data that yield the maximum subsidence (see the section above for a discussion of the leveling data and the very small movements expected at the leveling reference point). Similarly, only a representative selection of the subsidence curves obtained by axisymmetric modeling (i.e., from Figure 14) is included, noting that the variation in modeled subsidence trends during the first 28 yr of production from the reservoir is modest. Figure 15 also includes results obtained using 3-D analysis. The 3-D results are broadly similar to those of the axisymmetric analysis, confirming that excluding the asymmetries in the geological model has little effect on the general subsidence trend in the geomechanical models. This supports the authors' choice of investigating the sensitivity of model results to salt creep law through the use of simpler (and less expensive) axisymmetric runs.

Figure 15A plots the computed subsidence in meters. Here, one can see that, if a Young's modulus of 20 GPa is used for the reservoir rock (all curves shown apart from the gray one), then the time-evolution of field subsidence is initially followed rather well, but after 5 to 10 yr, the subsidence magnitudes are underestimated. This is the case for all salt models used. One way to increase subsidence magnitudes is to decrease the elastic moduli of the reservoir rock—that is, to make it less stiff. This is shown by the gray curve in Figure 15A. In principle, it is possible to match the subsidence observed in 2014 in this way, but doing so severely overestimates the initial subsidence response and also underestimates the rate of subsidence measured in 2014.

Figure 15B plots subsidence observations and model results normalized by the relevant subsidence value measured in February 2014 (the last leveling epoch that is analyzed here). The plot demonstrates that all finite element simulations, irrespective of salt model, predict that the subsidence rates would diminish due to the decreased pore pressure drawdown rate. It is clear that analyses that only include salt creep cannot reproduce the shape of the subsidence evolution curve—that is, cannot predict the higher subsidence rates observed in 2014.

On this basis, a major conclusion of the present study is that some other mechanism must operate (in addition to salt creep) that induces time-dependent subsidence in the field studied. It may be that the reservoir material behavior is not adequately represented as linear elastic with a constant modulus, as done here. For example, creep of the reservoir rock may occur. Alternatively, there may be permanent inelastic deformation or damage effects, which can lead to nonlinear stress-strain behavior (i.e., plastic yielding) and/or changes in elastic modulus with increasing effective vertical stress—and hence with progressive depletion through time (e.g., Pijnenburg et al., 2018, 2019). It might also be that other assumptions made here (e.g., on how compartmentalized or sealed from its surroundings the reservoir is) are violated. Exploration of these various alternative material models and assumptions requires data that were not available during the present study. An investigation into a number of such alternative models was presented by NAM (Nederlandse Aardolie Maatschappij, 2017).

Figure 16 plots cross sections through the observed subsidence bowl (as obtained from the two leveling traverses shown in Figures 5, 10) in normalized form at three different times. The corresponding 3-D model results (with linear salt creep) are added for the same locations and times. In this figure, there is barely any visible change in the normalized shape of the modeled or observed subsidence bowl with time. However, the width of the measured subsidence bowl (expressed, for example, as the distance between points exhibiting 50% of the maximum subsidence) seems to be less than that of the modeled subsidence bowl. Note also that, in both the north and south cross sections, the mismatch between the shape of the modeled and observed subsidence bowl is more pronounced to the east—that is, at positions with x larger than 190 km in the coordinate system used here.

This mismatch might be due to a number of reasons. It could be that the 3-D model reservoir (whose size was set on the basis of the results of a pore pressure analysis) extends too far to the east. Or it could be that the western and central parts of the reservoir have compacted more than its edges due to a more spatially concentrated reservoir pressure depletion there. Finally, it is possible that the subsidence profile

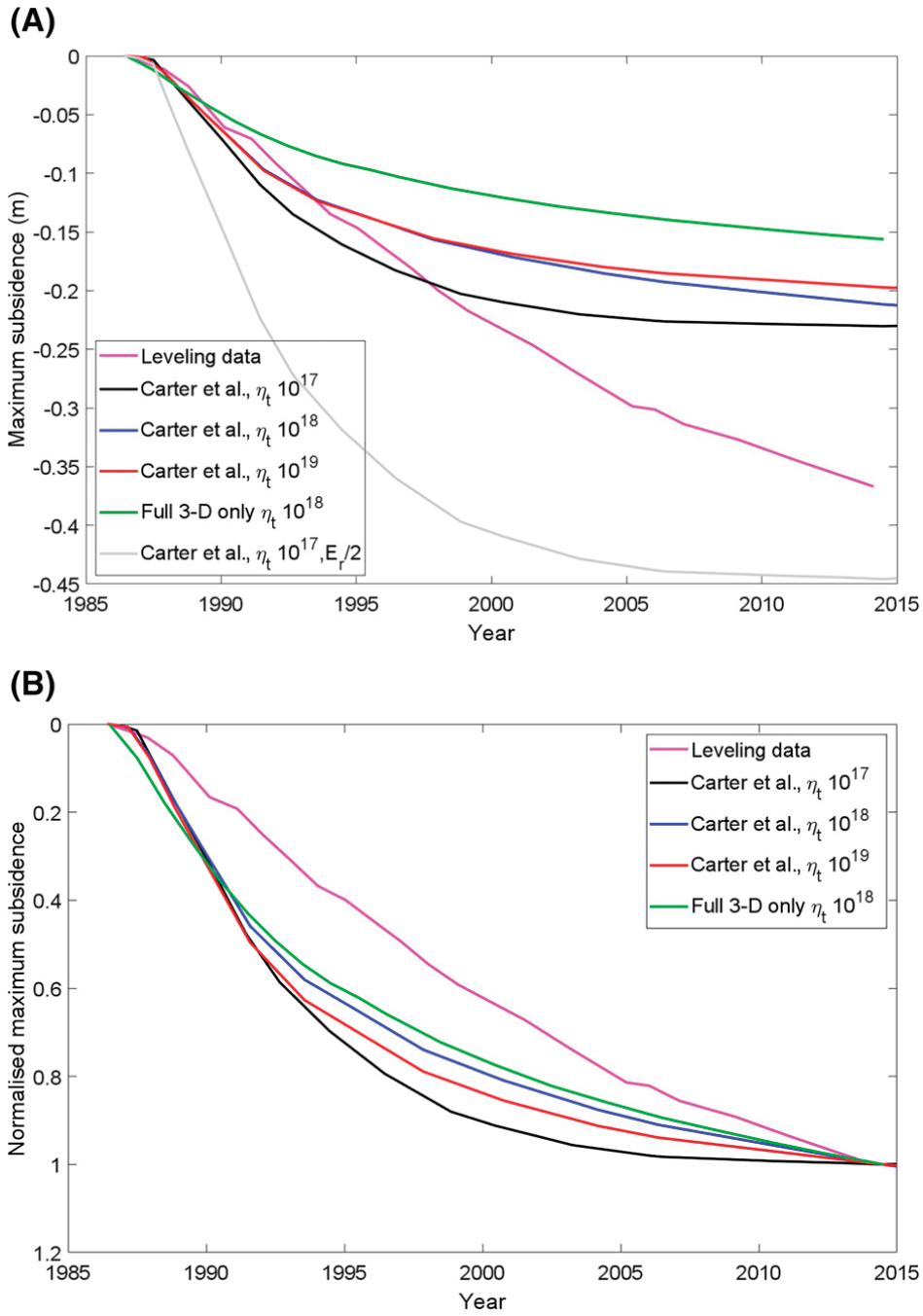

Figure 15. Axisymmetric and three-dimensional (3-D) model results for the evolution of maximum subsidence (i.e., the subsidence above the center of the reservoir), for a number of different rock salt models and taking E = 20 GPa, compared to leveling data for the point of maximum subsidence. (A) Subsidence in meters, including the result for a simulation in which the reservoir modulus was halved. (B) Subsidence values normalized with respect to the relevant subsidence value for February 2014, to aid comparison of evolution trends.

mismatch indicates that there is another mechanism by which subsidence develops. It is worth noting also that narrower than modeled ground settlement (subsidence) profiles are also a very common problem in finite element analyses of the similar problem of tunnel construction at shallower depths. Bym et al. (2013) discuss this and show that a method that does not constrain the ground to be linear elastic might offer a qualitative solution by reproducing narrower subsidence troughs, whereas Marketos (2018) shows that nonlinear soil material models reproduce well the smaller width of tunneling-induced settlement troughs.

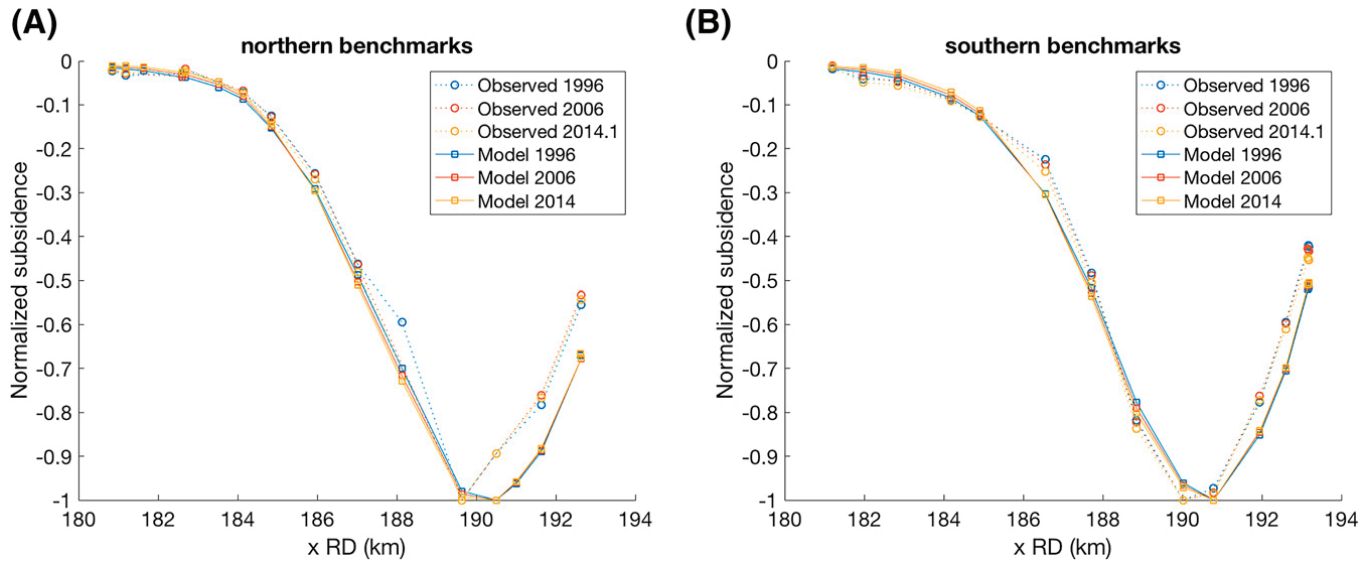

Figure 16. Subsidence bowl shape: three-dimensional model results (linear rock salt creep with a viscosity of 10^{18} Pa·s) for subsidence at three different times compared to the leveling data, along the (A) northern and (B) southern east to west measurement traverses (as shown in Figures 5, 10). All curves have been normalized by the relevant maximum subsidence value. RD = Rijksdriehoeksmeting, the national coordinates system of the Netherlands.

SUMMARY AND CONCLUSIONS

We show that reservoir pore pressure decrease data (the output of reservoir pore-fluid pressure analyses conducted by NAM) and measured maximum subsidence over the studied gas field are not linearly proportional to each other. Instead, measured subsidence increase rates have remained approximately constant, even though reservoir pore pressure depletion rates have decreased with time.

When assuming a linear elastic reservoir and including salt creep as the only mechanism causing time-dependent subsidence effects, the geomechanical model results cannot match the observed subsidence trends, irrespective of the salt creep constitutive model chosen. The mismatch increases toward higher levels of reservoir pore pressure depletion—that is, after the first decade of production. This indicates that there must be another mechanism that contributes to, or is responsible for, the observed time-evolution of subsidence. Good candidates for this additional mechanism include (1) inelastic reservoir rock behavior, characterized by stress-strain behavior showing a continuously decreasing hardening rate (e.g., due to plastic yield or decreasing elastic modulus); (2) creep of the reservoir rock; or (3) unexpectedly complex pore pressure equilibration behavior inside the reservoir and surrounding rock units—see Nederlandse Aardolie Maatschappij (2017).

This said, for the reservoir investigated, the current study shows that although salt flow does not change the volume of the subsidence bowl, and although its effects to date are already included in fitted subsidence models (see Nederlandse Aardolie Maatschappij, 2017), it does lead to significantly (up to 75%) greater maximum subsidence than calculated from unfitted, purely linear elastic analyses (see Figure 14). (Other work not reported here suggests that the exact value of the additional salt-induced subsidence depends on the size of the gas field, with larger fields being much less affected due to the relatively smaller volumetric proportion of salt affected by the shear stresses that develop close to the reservoir edges.) We also show that the magnitude of the effect of salt flow on the maximum subsidence and the timescale over which it occurs depend on the exact salt creep law used and the corresponding input parameters (including grainsize-dependence, for example), which are not tightly constrained and so add to uncertainties.

As many hydrocarbons fields worldwide are capped by salt (see, e.g., Grunau, 1981), the work reported here clearly has relevance beyond the present example. Creep of their salt top seals needs to be modeled carefully if subsidence predictions are required. Work shown also implies that salt flow may have significant effects in influencing the stress field evolution and fault (re)activation around salt-capped

reservoirs (see e.g., Orlić and Wassing, 2013; Buijze et al., 2017).

REFERENCES CITED

Bérest, P., B. Brouard, D. Brückner, K. DeVries, H. Gharbi, G. Hévin, G. Hofer, C. Spiers, and J. Urai, 2019, Very slow creep tests on salt samples: Rock Mechanics and Rock Engineering, v. 52, no. 9, p. 2917–2934, doi:10.1007/s00603-019-01778-9.

Breunese, J. N., R. M. H. E. van Eijs, S. de Meer, and I. C. Kroon, 2003, Observation and prediction of the relation between salt creep and land subsidence in solution mining—The Barradeel case: Proceedings, Solution Mining Research Institute Conference, Chester, United Kingdom, October 5–8, 2003, 20 p.

Buijze, L., P. A. J. van den Bogert, B. B. T. Wassing, B. Orlić, and J. ten Veen, 2017, Fault reactivation mechanisms and dynamic rupture modelling of depletion-induced seismic events in a Rotliegend gas reservoir: Netherlands Journal of Geosciences, v. 96, no. 5, p. s131–s148, doi:10.1017/njg.2017.27.

Bym, T., G. Marketos, J. B. Burland, and C. O'Sullivan, 2013, Use of a two-dimensional discrete-element line-sink model to gain insight into tunnelling-induced deformations: Géotechnique, v. 63, no. 9, p. 791–795, doi:10.1680/geot.12.T.003.

Carter, N. L., S. T. Horseman, J. E. Russel, and J. Handin, 1993, Rheology of rocksalt: Journal of Structural Geology, v. 15, no. 9–10, p. 1257–1271, doi:10.1016/0191-8141(93)90168-A.

Desbois, G., J. L. Urai, and J. H. P. de Bresser, 2012, Fluid distribution in grain boundaries of natural fine-grained rock salt deformed at low differential stress (Qom Kuh salt fountain, central Iran): Implications for rheology and transport properties: Journal of Structural Geology, v. 43, p. 128–143, doi:10.1016/j.jsg.2012.07.002.

Fokker, P. A., F. J. van Leijen, B. Orlic, H. van der Marel, and R. F. Hanssen, 2018, Subsidence in the Dutch Wadden Sea: Netherlands Journal of Geosciences, v. 97, no. 3, p. 129–181, doi:10.1017/njg.2018.9.

Gerya, T. V., 2010, Introduction to numerical geodynamic modelling: Cambridge, United Kingdom, Cambridge University Press, p. 260–261.

Govers, R., W. Drenth, and L. van de Wiel, 2014, GTECTON, technical manual: GTECTON developing team, 73 p.

Govers, R., and M. J. R. Wortel, 1993, Initiation of asymmetric extension in continental lithosphere: Tectonophysics, v. 223, no. 1–2, p. 75–96, doi:10.1016/0040-1951(93)90159-H.

Govers, R., and M. J. R. Wortel, 2005, Lithosphere tearing at STEP faults: Response to edges of subduction zones: Earth and Planetary Science Letters, v. 236, no. 1–2, p. 505–523, doi:10.1016/j.epsl.2005.03.022.

Grunau, H. R., 1981, Worldwide review of seals for major accumulations of natural gas: AAPG Bulletin, v. 65, no. 5, p. 933.

Hettema, M., E. Papamichos, and P. Schutjens, 2002, Subsidence delay: Field observations and analysis: Oil & Gas Science and Technology - Revue d'IFP Energies nouvelles, v. 57, no. 5, p. 443–458.

Houtenbos, A. P. E. M., 2011, Bodemdaling Waddenzee 1977-2011, accessed December 16, 2025, https://waddenzee.nl/publish/library/25/bodemd_houtenbos_dec2011.pdf.

Hunsche, U., and A. Hampel, 1999, Rock salt—The mechanical properties of the host rock material for a radioactive waste repository: Engineering Geology, v. 52, no. 3–4, p. 271–291, doi:10.1016/S0013-7952(99)00011-3.

Li, S., and J. Urai, 2016, Numerical modelling of gravitational sinking of anhydrite stringers in salt (at rest): Bollettino Di Geofisica Teorica Ed Applicata, v. 57, p. 233–246, doi:10.4430/bgta0178.

Marketos, G., 2018, Tunnelling induced settlements—Finite element predictions, soil model complexity and the empirical inverse Gaussian settlement curve: Proceedings of the 9th European Conference on Numerical Methods in Geotechnical Engineering (NUMGE 2018), Porto, Portugal, June 25–27, 2018, p. 1303–1307.

Marketos, G., R. Govers, and C. J. Spiers, 2015a, Ground motions induced by a producing hydrocarbon reservoir that is overlain by a viscoelastic rocksalt layer: A numerical model: Geophysical Journal International, v. 203, no. 1, p. 228–242, doi:10.1093/gji/ggv294.

Marketos, G., R. Govers, and C. J. Spiers, 2015b, Surface subsidence induced by hydrocarbons extraction, and the potential for time-dependent ground deformations: Proceedings of the 49th US Rock Mechanics/Geomechanics Symposium, American Rock Mechanics Association, San Francisco, June 28–July 1, 2015, 7 p.

Marketos, G., C. J. Spiers, and R. Govers, 2016, Impact of rock salt creep law choice on subsidence calculations for hydrocarbon reservoirs overlain by evaporite caprocks: Journal of Geophysical Research: Solid Earth, v. 121, no. 6, p. 4249–4267, doi:10.1002/2016JB012892.

Mossop, A., O. van der Wal, and R. van Eijs, 2011, Subsurface technical report: Subsidence modelling of Ameland Fields: Assen, the Netherlands, NAM Report, UIE Report No. EP201105208617, 36 p.

Munson, D. E., and P. R. Dawson, 1979, Constitutive model for the low temperature creep of salt (with application to WIPP): Albuquerque, New Mexico, Sandia National Laboratories Report SAND79-1853, 29 p.

Nederlandse Aardolie Maatschappij, 2017, Ensemble based subsidence application to the Ameland gas field—Long term subsidence study part two (LTS-II) continued study, accessed December 7, 2025, https://nam-onderzoeksrapporten.data-app.nl/reports/download/wadden/en/b2bb2626-2cf8-4d7f-994d-04a9995ebe9d.

Orlić, B., and B. B. T. Wassing, 2013, A study of stress change and fault slip in producing gas reservoirs overlain by elastic and viscoelastic caprocks: Rock Mechanics and Rock Engineering, v. 46, p. 421–435, doi:10.1007/s00603-012-0347-6.

Pijnenburg, R. P. J., B. A. Verberne, S. J. T. Hangx, and C. J. Spiers, 2018, Deformation behavior of sandstones from

the seismogenic Groningen gas field—Role of inelastic versus elastic mechanisms: Journal of Geophysical Research: Solid Earth, v. 123, no. 7, p. 5532–5558, doi: 10.1029/2018JB015673.

Pijnenburg, R. P. J., B. A. Verberne, S. J. T. Hangx, and C. J. Spiers, 2019, Inelastic deformation of the Slochteren Sandstone—Stress-strain relations and implications for induced seismicity in the Groningen gas field: Journal of Geophysical Research: Solid Earth, v. 124, no. 5, p. 5254–5282, doi:10.1029/2019JB017366.

Prij, J., 1991, On the design of a radioactive waste repository, Ph.D. thesis, University of Twente, Enschede, the Netherlands, 227 p.

Schléder, Z., and J. L. Urai, 2005, Microstructural evolution of deformation-modified primary halite from the Middle Triassic Röt Formation at Hengelo, the Netherlands: International Journal of Earth Sciences, v. 94, no. 5–6, p. 941–955, doi:10.1007/s00531-005-0503-2.

Spiers, C. J., P. M. T. M. Schutjens, R. H. Brzesowsky, C. J. Peach, J. L. Liezenberg, and H. J. Zwart, 1990, Experimental determination of constitutive parameters governing creep of rocksalt by pressure solution, *in* R. J. Knipe and E. H. Rutter, eds., Deformation mechanisms, rheology and tectonics: Geological Society, London, Special Publications, v. 54, p. 215–227.

Terzaghi, K., 1943, Theoretical soil mechanics: New York, John Wiley, 528 p.

Urai, J. L., Z. Schléder, C. J. Spiers, P. A. Kukla, J.-M. Lange, and H.-G. Röhling, 2008, Flow and transport properties of salt rocks, *in* R. Littke, U. Bayer, D. Gajewski, and S. Nelskamp, eds., Dynamics of complex intracontinental basins: Berlin Heidelberg, Springer-Verlag, p. 277–290.

Van Noort, R., H. J. M. Visser, and C. J. Spiers, 2008, Influence of grain boundary structure on dissolution controlled pressure solution and retarding effects of grain boundary healing: Journal of Geophysical Research: Solid Earth, v. 113, no. B3, B03201, 15 p., doi:10.1029/2007JB005223.

Van Thienen-Visser, K., A. G. Muntendam-Bos, and J. N. Breunese, 2015, Subsidence due to gas production in the Wadden sea: How to ensure no harm will be done to nature: Proceedings of the 49th US Rock Mechanics/Geomechanics Symposium, American Rock Mechanics Association, San Francisco, June 28–July 1, 2015, 9 p.

Verruijt, A., 1996, Complex variable solutions of elastic tunnelling problems: Delft, the Netherlands, Delft University of Technology, Geotechnical Laboratory Report, 73 p.

Verruijt, A., 1998, Deformations of an elastic half plane with a circular cavity: International Journal of Solids and Structures, v. 35, no. 21, p. 2795–2804, doi:10.1016/S0020-7683(97)00194-7.